J. Condensed Matter Nucl. Sci. 19 (2021) 198–216

Research Article

High Impedance Aqueous Solutions Improve CF/LANR Systems

Mitchell R. Swartz*

JET Energy Inc., Wellesley Hills, MA 02481, USA

Abstract

There are three reasons high impedance cold fusion/lattice activated nuclear reaction (CF/LANR) systems work so well—these are a high loading rate, intrapalladial deuteron flux, and a large cathodic increase of deuterons. This paper demonstrates the existence, and origin, of this cathodic increase of hydrogen isotopes from the applied electric field intensity. There results an advantageous spatial distribution of hydrogen between anode and cathode. This is another confirmation of the quasi-1-dimensional (Q1D) model of hydrogen isotope loading and further explains success of LANR activity using this configuration and technology.
 ISSN 2227-3123

Keywords: Cathode fall, Deuteron loading, Deuteron distribution, Hydrogen distribution, Metamaterial, Phusor®-type LANR cathode, Water, Cathodic hydroden increase.

1. Introduction to the Reasons for the Success of High Impedance CF/LANR Systems

This paper reviews the role of hydrogen isotope (deuteron) flow in excess heat (XSH)-active aqueous LANR systems [1–7], and in particular, it also explains exactly why these high impedance systems work so well. That is: What about the high impedance LANR aqueous system enables their incremental excess power gain and their time-integrated excess energy gain to be so far above the others.

Figure 1 shows the importance of using high impedance electrolyte in CF/LANR systems in two curves. They are the theoretical result of the Navier Stokes analysis [Eq. (2)] and the actual measured values of hydrogen ion concentration at five locations in the reaction chamber between anode and cathode of an alkaline ordinary water solution.

At first consideration, high electrical impedance (resistance) means low electrical currents, and that might seem antithetical to optimal loading of the palladium, but as shown below it is not. Normally, in an ordinary electrical circuit, increasing the impedance must reduce the net current, and that should decrease the deuterium flux in the Pd, but as shown below, it increases it. To demonstrate why this "paradox" operates here, two previously reported unique properties of high impedance CF/LANR systems are discussed [high loading rate and the intrapalladial deuteron flux] and then introduces the third important unique distinction of high impedance CF/LANR systems: their large cathodic

*Mitchell R. Swartz ScD, MD, EE, AC1ER, E-mail: drswartz@nanortech.com.

 ISSN 2227-3123

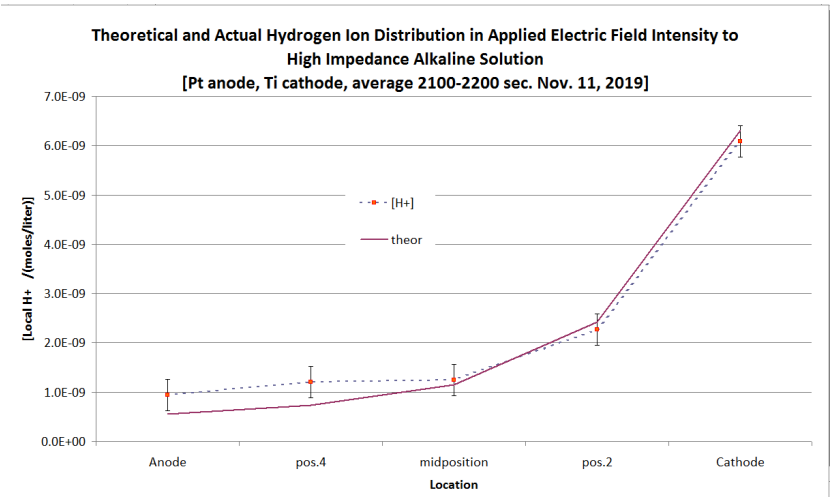

Figure 1. Comparison of An Electrically Driven Detected Cathodic Increase of Hydrogen with the Theoretical Derivation in mild alkaline ordinary water.

fall of deuterons. This paper reports experimental corroborations of the cathodic increase of hydrogen for a high impedance aqueous system and presents the results of three experimental runs which are confirmations of these Navier Stokes equations which predict, and clarify, the carrier flow in the solution, as well as the solution, itself, through the convective derivative. The results examine both spatially and temporally the hydrogen "cathode fall" which occurs in electrically driven aqueous CF/LANR systems. Classical electrochemistry refers to the term "cathodic fall" which describes what occurs as hydrogen (or deuterons) from the solution enters the cathode due to an applied electric field coming from the anode. In conditions such as discussed in this paper, however, there results a large hyperbolic increase in the hyperbolic pericathodic ("vicinal") concentration. Therefore, the term "cathode fall" has ambiguity, and can lead away from understanding the increase which occurs here, under these conditions. This paper uses the clear, more precise terms revealing the rise, increase, and the hyperbolic gain of the cathodic hydrogen concentration instead; retaining only with quotes the ambiguous term.

Figure 6 shows another "cathode fall" of hydrogen ions $[H^+]$. This figure shows a graph with three curves which present the aqueous hydrogen ion concentration at three positions in the reaction chamber between anode and cathode as a function of time (horizontal axis). Notice that at circa 5200 s an electric field was applied by putting a voltage between the anode and cathode. This was increased, and at 7000 s, the applied electric field is terminated. These two regions of time are marked by arrows.

It can be seen that the hydrogen ion concentration in the region of the cathode rises in time after the electric field is applied, but only until the electric field is terminated.

Figure 1 shows a graph containing two curves. These two curves are used to compare the expected value (by a theory, again being tested as hypothesis) and the actual measured values of hydrogen ion concentration at five locations in the reaction chamber, located between anode and cathode, in an alkaline ordinary water solution, at one short intervals in time. The measurements were taken within 1 min of each other, after being driven by an steady applied electric field intensity for ca. 20 min.

First, in Fig. 1, the solid curve is the theoretical expectation. The theory involves Eq. (2) to predict the actual measured values of hydrogen ion $[H^+]$ concentration. The theory and equations are from 1971, in the first discussion

of this theoretical derivation eventually used in the author's ScD thesis, and since elsewhere in the CF/LANR and oncologic literature, including this report. These calculations came from those theoretical derivations which are used to substitute for conventional electrochemistry requiring chemical equilibrium. Instead, with much more information, these equations lead to the quasi-1-dimensional (Q1D) model of loading [1].

Compared to the solid curve, the dashed curve which is from the measured data points obtained during the interval of 2100 to 2200 s after initiating the applied electric field intensity between the electrodes.

Second, note that Fig. 1 does indeed clearly show a "cathode fall" of pH resulting from the rise in hydrogen ion concentration. This is a euphemism to describe the applied electric field intensity producing a local increase (a "rise") of proton (or deuteron) concentration vicinally before the cathode. This cathode increase of hydrogen isotope is important. It enables stable engines of excess heat with gains in the range of 200%–500% and more, in response to an applied electric field. The diameter of the pH meter, or the separator are not taken into account because they are not relevant to first order since the pH meter gives the local $[H^+]$ concentration directly. Some stirring must have been present from the movement of the linear actuator moving the pH electrode's head through the water, from cathode to anode and back and form, so a small pause was used. Bubble was never significant in comparison. It also was not expected to obscure any significant part of the cathode since the area was so large (see Fig. 5). This system generated much information, including that used for the curves in Figs. 1 and 6. These systems have been used to drive both Stirling engines and Peltier devices (to generate electricity) at over-unity compared to input power levels [3–16].

The important point is that these are corroborations, and further direct experimental evidence of the importance, of the electrochemically useful Navier Stokes equations derived by the author circa 1971 [17]. These have successfully predicted the existence of, including the shape and form, the hydrogen/deuteron cathodic increase in concentration in ordinary and heavy water solutions to an applied electric field intensity. In 1989, these Navier Stokes equations were later expanded specifically for LANR using Q1D [1–3] which were thereafter explored and expanded [2–6]. By the mid-90s, meticulous parametric CF/LANR experiments made both solution impedance, and the type of ion in the cell, as the independent variables [5]. These equations, and engineering, have been successfully used in cold fusion [3–16,18–33] and antimicrobial, antiviral, and antineoplastic therapy [34–47].

Third, another important point is the qualitative match to the theorized result predicted by the theory, and used (also successfully) in the Q1D model of flow in CF/LANR. That theory has resulted in many active CF/LANR cells, components, and has led to many discoveries. The take home message is that the application of this LANR/electrical engineering has also led to novel devices, active samples, and discoveries in the optical antiStokes [28–30] and Deuterium-line RF radio regions [31–33].

2. Background

2.1. Successful LANR requires electrical engineering

Drs. Fleischmann and Pons first reported excess energies of 4 MJ (megajoules) in 80 h. Today, several LANR devices show excess power gains from 25% to 80 times input electrical power, beyond the controls. Taking advantage of Navier Stokes equations and other LANR engineering, aqueous high impedance LANR devices have shown power gains 200%–400%, and one has yielded circa 8000% power gain for a short time. JET Energy has shown that some cathodic electrodes, of specific shape, are metamaterials which produce excess heat of a superlative magnitude, successfully driving Stirling engines at the 19+ W level. They run in both open and closed systems, and driving motors, with on-line monitoring, redundant, high precision, time-resolved semiquantitative calorimetry [8,4,7]. Shown at ICCF-10 at MIT, Cambridge, MA, August 03, the JET Energy Inc. CF demonstration system produced excess heat over five days. Videos and other data were shown to hundreds of visitors demonstrating how this system is different from other systems. The energy gain was ~2.7 in 2003.

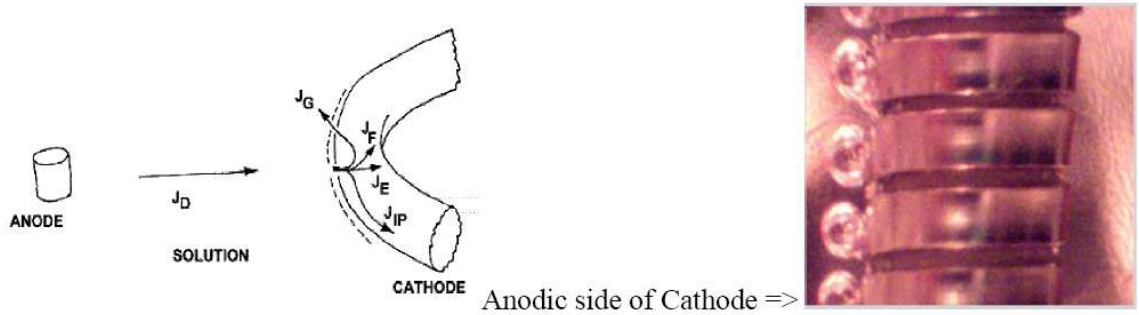

Figure 2. Schematic Model of Deuteron Flux and PHUSOR®-type Metamaterial. (*Left*) a schematic, simplified, representation of the anode, solution, and a portion of the cathode along with five types of deuteron fluxes involved in loading, D_2 evolution, and putative fusion; in solution and the palladium. (*Right*) A close-up of an active Phusor®-type spiral-wound excess-heat-producing palladium cathode. It is in a high impedance aqueous solution, and the anode is to its left and is not shown. These deuteron fluxes include entry into the metal (J_E), movement to gas evolution (J_G), and an extremely tiny loss by potential fusion reactions (J_F). There is conservation of deuterons with the exception of a loss (J_F) to all putative fusion reactions, which are extremely small, if present. There is a continuous, equilibrium, flux of deuterons within the cathode (J_{IP}), which may be consistent with excess heat and an observed unusual bubbling pattern seen routinely in high impedance active aqueous LANR systems.

2.2. Mathematical analysis of deuteron flow (flux)

Deuterium fluxes in palladium systems need further study. Nernst calculations of the activities of electrolyte [48,49] adjacent to a metal electrode have been applied to LANR to derive distributions of deuterium in the palladium and solution. However, the LANR systems are simply not at equilibrium, and Nernst calculation may not be applicable [1]. Also, a vicinal reference electrode may herald the Nernst potential, but probably not the loading flux rate (which will be shown below to be key to these reactions).

Therefore, a Q1D model for hydrogen loading of an electrode was formulated [1], which does not require equilibrium for accuracy. This was designed based on Navier Stokes calculations which predict the hydrogen distribution in these aqueous high impedance LANR systems. The Q1D model describes the loading flux of hydrogen by the ratio of two energies (electric order to thermal disorder ratio).

2.2.1. *Localized, limited-area, large-bubble coverage (asymmetric electrolysis)*

Deuteron flux (J_D) begins far from the cathode surface, in the deuterium oxide (heavy water) located between the electrodes, where the deuterons are tightly bound to oxygen atoms as D_2O. There is no additional solute. In the absence of significant solution convection, the flux of deuterons (J_D) results from diffusion down concentration gradients and electrophoretic drift by the applied electric field [1,4]. Cationic deuteron flux (J_D) brings deuterons to the cathode surface, from the heavy water as D-defects [50–56] are driven by the applied electric field intensity to create a cathodic fall and double layer before the electrode surface.

From the metallurgical point of view (POV), from the metal surface, atomic deuterons either enter the metal ("are loaded"), remain on the surface, or form diatomic deuterium gas bubbles (D_2). The gas bubbles (D_2) are undesirable producing low dielectric constant layers in front of the electrode, obstructing the electrical circuit.

2.3. The first reason for success of high impedance solutions: loading efficiency

Figure 2 also shows a close-up of an active Phusor®-type spiral-wound excess-heat-producing palladium cathode. The Pt anode is to the left of the cathode, and is not shown in the photograph, as discussed in detail [9]. A high

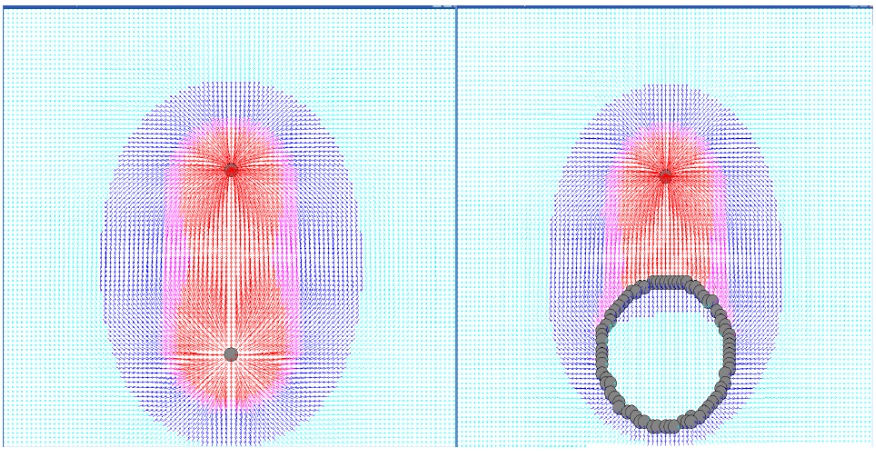

Figure 3. Electric field distributions for wire-wire and wire-Phusor®-type system.

electrical resistivity solution, located between the two electrodes, bathes the metamaterial cathode, including within the spiral. There is seen very limited, well localized, small area large-bubble (asymmetric) coverage bubbling vs. normal bubbling. There are bubbles only on one side of the cathode, what we call "asymmetric bubbling" which differs from normal bubbling. In this high voltage system (~1500 V), videos (including those shown at ICCF-10 of which the above figure is a single frame grab) demonstrated that cathodic electrolysis bubbling occurs, if the conditions are appropriate, almost solely on the anode-side (left-hand portion of the spiral wound cathode in the photo) of this PHUSOR®-type heating electrode system.

"Asymmetric electrolysis" heralds, and drives, intrapalladial deuteron flux deuteron flux through that portion of the loaded metal cathode. Thus, it is a sign of LANR success for some excess-heat-producing cathodes as experimentally observed and reported, and openly demonstrated at ICCF-10 [9,13,15]. Figure 2 demonstrates this important finding of this system - asymmetric electrolysis which is seen on only one side of the cathode (which is facing the anode). It heralds the forced movement of the loaded deuterons through the loaded metal. This creates a deuteron current through the palladium electrode, and an improved likelihood of success in LANR.

2.4. Derivation of the hydrogen or deuteron distribution

In the absence of significant solution convection, molecular flux (F) also results from both movement of deuterons [D(z,t)] down concentration gradients and from electrophoretic drift in the applied electric field. The deuteron flux, J_D, depends on deuteron diffusivity (B_D) and electrophoretic mobility (μ_D), and the applied electric field intensity (the gradient of the potential)

$$J_D = -B_D \frac{d[D(z,t)]}{dz} - \mu_D [D(z,t)] \frac{d\Phi}{dz}. \quad (1)$$

In this zeroth order model, consideration is not made for reduction of hydrogen at the cathode (loading and/or gas evolution). That is done in Q1D model of loading [1], and subsequent improvements [2,3]. It is assumed that all electrical reduction occurs at the cathode.

Thus, in the steady state, the final spatial distribution for hydrogen (or deuterons) is

$$D(z,t) = \frac{IE_R/(AF)(\sqrt{K_0/D})\sinh(\sqrt{(K_0/D)})Z\}}{\cosh(\sqrt{K_0/D})L - 1} \tag{2}$$

where I is the electrical current; E_{R} is the efficiency of electron transfer to the hydrogen isotope (electrical reduction); A is the area of the electrode; F is the Faraday; K_{o} is the oxidation rate in the bulk; and D is the diffusivity of the hydrogen isotope. The coefficient of the hyperbolic term is of the form A/(B (cosh(A)-1)). Therefore, L'Hospital's rule may be used to determine the limit as $K_{\mathrm{o}} \rightarrow$ infinity (i.e. fast reoxidiation).

2.5. Results: loading rate equation derived from diffusion equation

From the concentration polarization of deuterons before the cathode, the Pd loads, controlled by the double layer, which limits the entry of deuterons to the metal surface. At the inner boundary of the double layer, intermolecular deuteron transfer from the heavy water solution to the metal surface, coupled by electron-limited transfer, leaves an atomic deuteron on the metal surface. This leaves an atomic deuteron attached to the metal surface, and the electrode metallurgy controlled by the tiny interfacial region, which might be less than 10 Angstroms thick, by the applied electric field intensity, and by the local concentration of deuterons. The entry mechanisms to the palladium surface are driven by infrared vibrations and microwave rotations [50,51], creating solution photosensitivity reactions producing a photoactivated increase of excess energy and loss of power gain [13].

Palladium has its surface populated with atomic (D) and diatomic deuterium (D_2). A large number of those deuterons can also enter the metal forming a binary alloy. Deuterons which enter (load) into the palladium lattice are "dressed" by a partial electronic cloud, shielding their charge (Born–Oppenheimer approximation). The deuterons drift along dislocations and through the lattice and its vacancies, falling from shallow to deeper located binding sites. There is obstruction by ordinary hydrogen and other materials at interfaces and grain boundary dislocations.

2.6. The deuteron flux equation proves that successful LANR is not electrolysis

Dividing each flux by the local deuteron concentration [D(z,t)] yields the first-order deuteron flux constants, k_{E}, k_{G}, and k_{F} (cm/s), respectively. These involve entry of deuterons to the electrode, to the gas phase, and to successful fusion. They are the basis of the rest of Eq. (3).

$$k_{\mathbf{E}} = (\mu_{\mathbf{D}} E) - (k_{\mathbf{G}} + k_{\mathbf{F}}). \tag{3}$$

Equation (3) is the deuteron loading rate equation. It relates cathodic deuteron gain from the applied electric field to the loss of deuterons from gas evolution and fusion and teaches many things.

Note especially that as shown in Eq. (3), that another real difference distinguishing high impedance systems in CF/LANR is through the impact of the applied electric field intensity. In high impedance systems, E with be larger, and therefore the loading flux rate (k_{E}) will be as well.

The deuteron loading rate equation shows that the deuteron gain of the lattice (through the first order loading flux rate (k_{E})) is dependent on the applied electric field MINUS the flux rate losses of deuterons from gas evolution (k_{G}) and fusion (k_{F}). The deuteron loading rate equation, Eq. (3) reveals that desired LANR reactions are quenched by electrolysis, which is opposite conventional "wisdom" that LANR is "fusion by electrolysis." The other name for CF/LANR being "fusion by electrolysis" is a misnomer. Equation (3) also heralds that LANR can be missed by insufficient loading, contamination (effecting k_E, by protons or salt), and by the evolution of D_2 gas, which all inhibit the desired LANR reactions, and lead to the optimal operating point manifolds.

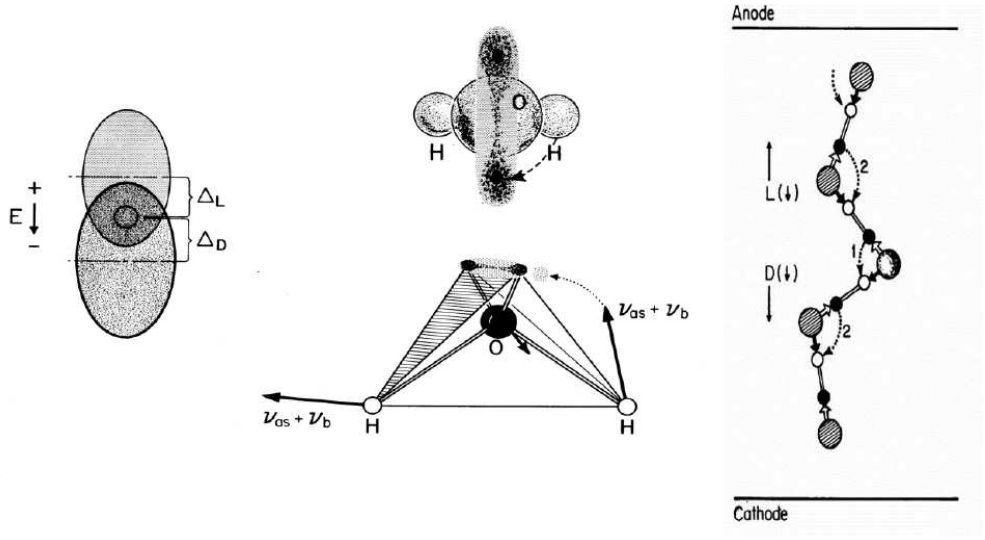

Figure 4. Infrared deuteron transfer L- and D-proton transfer. (*left* The large dielectric permittivity of water results from the fact that an applied electric field intensity produces the drift ellipsoids of hydrogen and "holes" where there is the absence of a proton (or deuteron in heavy water). (middle) Here, an infrared vibration launches a proton from one site on an oxygen electron orbital to another site. This creates a paired of defects (one O–O bridge with two hydrogens, and the other with none; the L- and D-proton defects). (*right*) Here there is a series of proton transfers resulting from the first infrared deuteron transfer. The resultant L- and D-proton defects initially arising from that infrared vibrations move through the oxygen lattice and generate the drift ellipsoid shown on the left-hand side.

The modified deuteron flux equation is Eq. (4) changed by substituting the Einstein relation, which makes for an equation reminiscent of semiconductor physics at p–n junctions. The first term now has geometric, material factors (L is length; B_{D} is the electrophoretic mobility), and the ratio of two energies (the applied electric energy $[q * V]$ organizing the deuterons divided by $k_{\mathrm{B}}{}^{*}T$, thermal disorder). The second terms are the first-order loading flux rates for deuteron entry and gas loss.

$$k_{\mathrm{E}} = \frac{B_{\mathrm{D}} qV}{L * k_{\mathrm{B}} T} - (k_{\mathrm{G}} + k_{\mathrm{F}}). \tag{4}$$

The Q1D models most important insight is that the first-order D-flux equation, with the substitution of the Einstein relation, shows that the ability to load D depends on the ratio of ordering energy, (the applied electric field) to thermal disorder ($k_{\mathrm{B}}{}^{*}T$) minus what goes up into the gas. The latter is perhaps most important because it reveals why so many have failed to generate successful LANR.

Thus, the modified deuteron flux equation reveals how competitive gas evolving reactions and the applied electric field energy to thermal energy ($k_{\mathrm{B}}{}^{*}T$) are both decisive in controlling the deuteron loading flux in palladium. Successful LANR experiments are dominated by this ratio reflecting the "war" between applied electrical energy which is organizing the deuterons versus their randomization by thermal disorganization. The two terms are the first-order deuteron loss rates by gas evolution and the desired fusion process(es).

It is ironic that the modified deuteron flux equation is similar to one of the equations of an intrinsic semiconductor, but the methods of proton/deuteron movement through water, discussed below, are not. However, in both cases, the Navier Stokes equations and continuum electromechanics are applicable.

2.6.1. *The second reason for high impedance success: intrapalladial flux from metamaterials such as the PHUSOR®-type metamaterial technology*

Metamaterials [4,6,7] and deuteron-loaded Group VIII alloys that exhibit "lattice assisted nuclear reactions" (LANR) have surprising, physical characteristics that defy earlier expectations, yet each produce solid, indelible experimental results. Metamaterials, through their unique, novel structures, can make previously "impossible" effects occur. Conventional metallurgy and material science accrue from the "internal structure of cathode material," whereas metamaterials result from the precisely crafted and planned external structure. Their precisely engineered materials and structures have characteristic behavior far beyond what is normally expected, making previously "impossible" effects such as negative refractive index and electromagnetic cloaking occur. Similarly, reports of excess energy and nuclear reactions from solid-state LANR [25–42] were initially felt to be impossible, but growing experimental evidence suggests otherwise. Active LANR devices produce helium-4 and tritium as nuclear ash, with both very small amounts of emissions, and hundreds of thousands of joules of "excess heat" per day.

The uniquely shaped spiral Phusor®-type cathodic structure has stood out for reproducibility, activity, and power gain, for several Group VIII materials. Its arrangement and stereo-constellation of electrodes appears to be one of the better arrangements for an LANR system, measured by activity and power gain [4–9]. We previously reported that unique well localized, small-area bubble coverage has been correlated with successful LANR-active Pd/D_2O/Pt, Pd/D_2O/Au, and Ni/D_2O,H_2O/Pt Phusor®-type devices operation. This has been confirmed by heat flow measurement, calorimetry, electrical, and mechanical energy conversion devices, and dual serial calorimetry. This type of LANR device, with its helical, cathodic design and low electrical conductivity solution, is the most successful half-electrochemical system we have found judged by robust excess heat production and reproducibility. Why?

2.6.2. *Distinguishing E-fields of PHUSOR®-type metamaterial technology*

The Phusor®-type LANR device is a metamaterial and its physical structure enhances the metallurgic properties of loaded palladium. This metamaterial change alters the electric field distribution, producing continuous deuteron flux within the loaded palladium. This is unique to this device creating a distinguishing electric field (E-field) distribution different from customary wire–wire, and other systems. Our hypotheses for this aspect of its superior function included the cold working, the preparation, Frenkel defects, and the possibility of specific alterations in the electric field intensity distribution. Although classical electrostatics analysis indicates that a perfect conductor does not have an electric field within it, the real palladium cathode is not a perfect conductor. We measure the palladium electrical conductivity by four terminal measurements which, for these Phusor cathodes, range from 40 to $\sim$ 120 mΩ.

A unique E-field distribution can be generated to provide intra-palladium deuteron flux, linked to successful LANR results. In Fig. 3, in the first configuration (*left*) shown, the electric field intensity for two parallel, infinitely long, electrodes (anode and cathode). What is shown is the cross-section electric field intensity distribution between two electrodes; so that the wires only appear as two circles. The electric field intensity is shown in two dimensions, and in a plane which is located perpendicular to the direction of the electrodes which are oriented in a direction coming out of the figure. The length of the vector is proportional to the magnitude of the electric field intensity. The direction of the vector of the electric field intensity is shown by a circle at the end of each line. Between the electrodes, the direction of the electric field intensity points from anode to cathode. At the electrodes, the electric field intensity is directly perpendicular to the each electrode. There is no tangential electric field, consistent with classical electrostatics.

By contrast, the Phusor®-type LANR metamaterial design with its spiral cathode system-wire anode system, with its open helical cylindrical geometry, creates a unique and unusual electric field distribution superior in performance. This is seen in the second configuration in Fig. 3 which shows the electric field intensity, in a cross-section, between

a spiral cathode metamaterial-shaped Phusor-type component which is electrically polarized against, and physically located opposite, an anodic wire of platinum. In cross-section, the Phusor®-type LANR component is schematically represented as only its thickness, with the more complex structure approximated as a distributed cathode in the shape of a circle here, which is actually a curved spiral.

In Fig. 3, on the right-hand side, again there are regions near the cathode where the electric field intensity is completely normal (perpendicular) to the cathode. However, what is different, and novel in this case, is the presence of an electric field intensity within the metal, creating a flux of isotopic hydrogen within, and through, the electrode. There does occur an entirely different distribution of the electric field intensity. The shape of the structure effects the outcome as much as the material, which is the characteristic of a metamaterial. As a result, two types of deuteron flows are created by the Phusor®-type LANR metamaterial cathode. The first is the standard deuteron interelectrode (between electrodes) loading flux, beginning in the solution and ending in the metal lattice, driven by the applied electric field intensity. The second is an additional intraelectrode deuteron flux, through the metal, itself. This additional type of deuteron flow is critical and enables superior LANR results ("high activity").

The Phusor®-type-LANR generated metamaterial-derived intrapalladial flux into the cathode is heralded by small bubble evolving area on the surface of palladium and linked to activity of LANR cathodes (Fig. 2).

In summary, geometry, stereoconstellation, and location of electrodes, metamaterial issues, are now shown to play additional possible roles in successful LANR experiments. This intraelectrode palladium flux is necessary to produce the desired reactions and that such a flux is often missed in competing, less efficient with respect to producing "excess heat"-systems.

2.7. Background

2.7.1. *Water's structure enables intramolecular H movements*

"One of his hobbies ... photographing how cannonballs are stacked on different courthouse lawns. Apparently how they've got them stacked in that picture is very unusual." – Kurt Vonnegut, "Cat's Cradle"

For most materials only the electronic and ionic polarization are significant, and, therefore, the dielectric constants of almost all materials are usually in the range of 3–6. However, for water, and Ice1_h, the arrangement of the molecules permitting proton disorder in the sublattice introduces a new method of electric conduction and polarization, and the result is a much larger dielectric constant; a whopping 92 for ice, and 88 for water. Before going further, it is extremely important to recognize that water is essentially ice. Only a small fraction of the hydrogen bonds are broken. Very few. This is demonstrable by considering the ratio of the heat of melting plus the specific heat to room temp (or whatever) to the that sum plus the heat of boiling which indicates that most of the hydrogen bonds are intact. This degree of bonding is expected because the energy of the hydrogen bond is 4.5 kcal/mol and room temperature $k_B * T$ would not impact that. The importance, and it cannot be said enough, is that these ice structures and charge carriers discussed below are the origin of the high permittivity of water (which is why we are here).

This unusually large dielectric constant of water distinguishes it from most other materials, and enables it to be an exceptional solvent and enable diverse reactions ranging from chemical solvation to free radical reactions, which can then occur by shielding free charge and unpaired electrons, respectively.

It is water/ice's proton disorder and the drift of defects which decrease that disorder, which creates the unusual dielectric properties of water. The high dielectric constant of water actually results from movements of protons in the proton sublattice. This is created by the electric field-directed movement of defects [50,51]. Thus, the origin of this unique feature of water/ice arises from the electrical response of water to an applied electric field intensity.

2.7.2. *Water's migrating L- and D-defects produce electrical conductivity and a large dielectric constant*

Normally, there is one proton between each pair of oxygen nuclei (Fig. 5), but not always. L and D defects arise from infrared vibrations, as suggested by Bjerrum [55,56]. They occur because normally there is one proton between each pair of oxygen nuclei. A D-defect has two protons-between any two oxygen nuclei. An L-defect has none. This D-defect conduction/polarization process augments other charge carriers, ionic drift, space charge polarization, and clathrates.

At any molecular site across the heavy water solution, the applied electrical energy is a tiny fraction compared to $k_{\mathrm{B}} * T$, so the deuterons migrate by drift ellipsoids of L- and D-deuteron defects in the applied electric field creating a ferroelectric inscription [50,51]. With the background thermal energy thus creating L and D defects throughout the volume of water or ice, the action of an applied electric field intensity to a sample of water/ice results in a drift of these intramolecular proton (and deuteron) defects within the proton sublattice. The movements inscribe-into that proton sublattice—a generally field-directed electric dipole moment. Intramolecular proton/deuteron transfer in lattice bound water molecules yields very large permittivities in organized lattices. The resultant D-defect migration also produces a "cathodic fall" of deuterons and an E-field contraction so that most of the voltage drop is at the interface in front of the electrode surface. This concentration polarization may produce very large local electric field intensities, possibly ranging from 10^4 to 10^7 V/cm.

2.7.3. *Water's structure enables inscribed ferroelectric moments*

The result of an applied electric field is that it inscribes a series of intramolecular defects within the water lattice (Fig. 4). Very relevant to CF/LANR, the applied electric field intensity thus offers two methods of proton transfer to the cathode. There is the conventional drift of the ions and there is possible propagation of the L- and D-defects for loading. What is not appreciated generally is that such intramolecular proton/deuteron transfer in lattice bound water molecules is what yields very large permittivity in organized lattices. Over vast distances, the L- and D-defects migrate in an applied electric field intensity. The normal spheroids of defects distort into field-directed ellipsoids, which are shown. As the defects migrate, they leave trails of proton order which are slowly erased by thermal action.

The inscribed defects create a large electric dipole moment. It is this electric dipole moment which creates the large dielectric constant. Drift ellipsoids of the defects inscribe a ferroelectric imprint into the water; they inscribe a domain until thermal processes eventually erase it. This ferroelectric inscription has several important implications. First, when water is polarized there is a measured, very large dielectric constant ($\sim$95) which is not necessarily a value applicable on a molecular level, for reasons discussed above. Intramolecular proton/deuteron transfer in lattice bound water molecules yields very large permittivities in organized lattices.

3. Experimental

3.1. Measuring the hydrogen isotope distribution

A system was 3D printed to measure the cathode fall as a function of applied electric voltage and to determine how closely the result was to the original theoretical prediction [17]. The 3D-printed system was fitted to a pH electrode holder attached to a linear actuator driven by a byj48 stepper motor run by an Arduino sketch. The program (attached as Appendix) was designed to move the sensor in a series of repeatable steps between the platinum wire anode and the larger titanium cathode, and to take and log pH measurements at each location, repeatedly over time. That cathode is seen next to the pH electrode in the photograph shown in Fig. 5. The electrical driving system was put on after a control time, and then stopped.

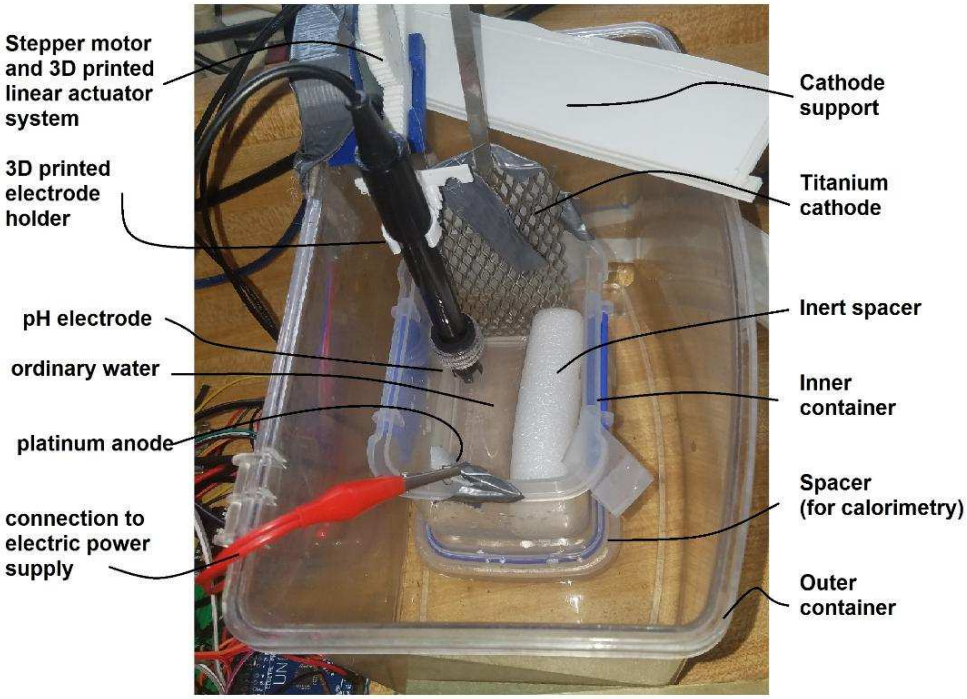

Figure 5. Physical setup to derive and detect a hydrogen cathodic increase over time.

Figure 5 shows the experimental setup used to measure the changing "cathodic fall" over time. The figure shows two containers, a pH electrode, and two electrodes (although the anode is less easy to see than the wire connection between it and the electrical power supply). The 3D-printed pH holder and linear actuator driven by the byj48 stepper motor and ULN2003 stepper driver was used to successively, and repeatedly, move the sensor between the platinum wire electrode and the large titanium cathode (vicinal to the pH electrode in the photograph).

The diameter of the pH meter, or the separator are not taken into account because they are not relevant to first order since the pH meter gives the local [H+] concentration directly. Some stirring must have been present from the movement of the linear actuator moving the pH electrode's head through the water, from cathode to anode and back and form, so a small pause was used. Bubble was never significant in comparison. It was also not expected to obscure any significant part of the cathode since the area was so large (see Fig. 5).

This system generated much information, including that used for the curves in Figs. 1 and 6.

4. Results

4.1. The third reason for high impedance success: hyperbolic cathodic increase of hydrogen

The linear actuator pH measurement system generated the information in Figs. 1 and 6. Figure 6 shows another "cathode fall" of hydrogen ions [H+]. This figure shows a graph with three curves which present the aqueous hydrogen ion concentration at three positions in the reaction chamber between anode and cathode as a function of time (horizontal

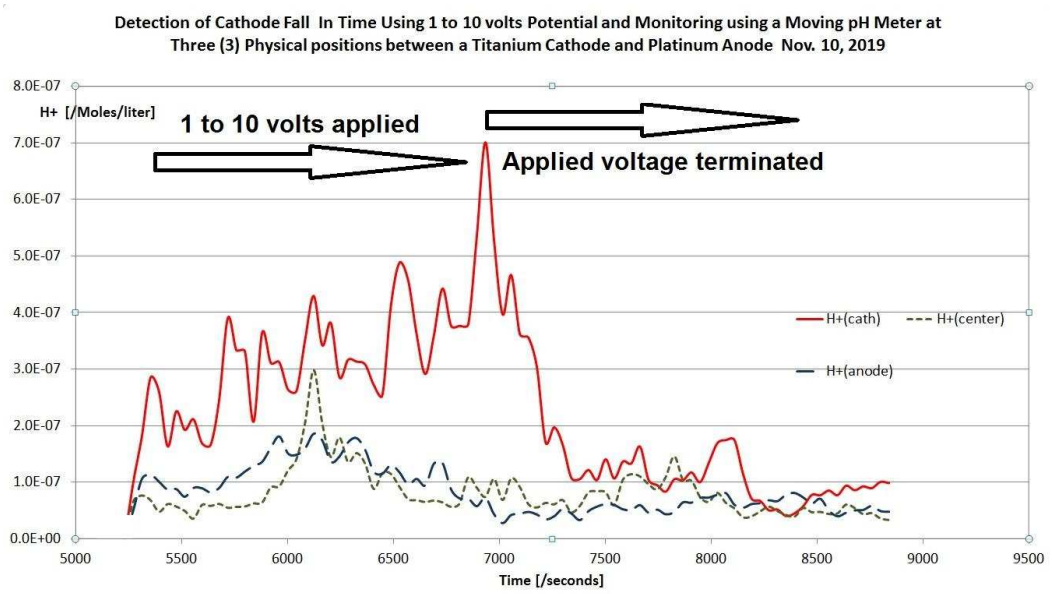

Figure 6. Detected cathodic increase of hydrogen (solid line). Shown are the results of an ordinary water solution. Shown are the results at three different locations between anode and cathode, made sequentially during the experimental run. The rising applied voltage was terminated, as shown.

axis). Notice that, at circa 5200 s, an electric field was applied by putting a voltage between the anode and cathode. This was increased, and at 7000 s, the applied electric field is terminated. These two regions of time are marked by arrows.

It can be seen that the hydrogen ion concentration in the region of the cathode rises in time after the electric field is applied, but only until the electric field is terminated.

5. Conclusions

5.1. Three reasons for the success of high impedance aqueous LANR systems

(1) There are (at least) three reasons why high electrical impedance aqueous CF/LANR systems do so well. First, as demonstrated by Eq. (3), the differences distinguishing high impedance systems in CF/LANR began through the impact of the applied electric field intensity with the solution containing an isotope of hydrogen, deuterons in the most important case shown previously in high impedance aqueous CF/LANR systems, the applied E-field drives the loading of the cathodic palladium, characterized by the loading flux rate (k_{E}). The loading is driven by the intensity of the E-field, and this is the first advantage favoring high impedance CF/LANR systems. Second, another difference distinguishing high impedance systems is the generation of deuteron flux through the palladium. This is a metamaterial action in LANR, using these novel hydrogen energy-production solid-state systems; a new spectrum of devices using intraelectrode deuteron flow.

Third, this report is an another experimental confirmation of a theoretical expansion of the Navier Stokes equation involving the Q1D model of hydrogen isotope loading. The results here demonstrate clearly that deuterons to pile up near the cathode in high impedance aqueous CF/LANR systems. This is a MAJOR change

in proton/deuteron distribution. In the applied electric field intensity, the deuterons assemble in a cathodic increase from regions throughout the aqueous volume, with the greatest deficit occurring at the anode. Thus, this paper demonstrates the existence, and origin, of a cathodic increase of hydrogen isotopes from the applied electric field intensity for high impedance aqueous solutions. But there is more: most importantly, there results an advantageous spatial distribution of hydrogen between anode and cathode. This is because deuteron (or hydrogen) amplitude (concentration height) always effects diffusion though a metal, material, or cathode (e.g. by Fick's law, which is one important methods how we measure PO_2 in the hospital or laboratory). The MOST important result is the relatively high concentration of deuterons vicinal to the cathode which promotes high concentrations at the cathodic double layer and therefore the highest possible loading of both the near-surface and bulk regions of the cathode. Future studies should also examine the role of solutes on the resultant distribution through changes in Benard instability [57].

(2) Other lessons have come from these efforts. This is another confirmation of the Q1D model of hydrogen isotope loading and further explains success of LANR activity using the metamaterial PHUSOR-type cathodic configuration and high electrode impedance technology.

(3) Looking forward, the key to the successful design and engineering of many energy systems ultimately depends on recognizing the structure and properties of water, its deuteron or proton sublattice, and its relatively unique dielectric response to the application of an electric field intensity yielding the requisite cathodic increase of deuterons/protons. The successful design and engineering of an energy production system ultimately depends on recognizing the structure and properties of water and its relatively unique dielectric response. Those who work with cold fusion and energy systems involving water ought to consider these processes as well, because they impact the proton disorder itself of water and ice, and LANR activity, itself.

Acknowledgments

The author gratefully acknowledges and thanks Gayle Verner, David Nagel, Alex Frank, Isidor Straus, Marcus Zahn, Brian Josephson, and Steven Senturia, and Joshua Gyllinsky for their very helpful comments, editorial assistance, critique, ideas and suggestions. The author is grateful to the late MIT Professor Arthur von Hippel and William Westphal for their help in understanding the dielectric and transconduction properties of water/ice, and to Louis Smullin for permission to release the figure shown in Figure 4 created by John Mara. This effort has been supported by JET Energy Inc., Nanortech Inc., and Anthropocene Institute, LLC.

References

[1] M. Swartz, Quasi-One-Dimensional Model of Electrochemical Loading of Isotopic Fuel into a Metal, *Fusion Technol*. 22 (2)(1992) 296–300.

[2] M. Swartz, Isotopic Fuel Loading Coupled to Reactions at an Electrode, Proc. ICCF4 2, (1993), p 429; Fusion Technol., 26, 4T, 74-77 (1994); www.lenr-canr.org/acrobat/EPRIproceedinga.pdf

[3] M. Swartz, Codeposition Of Palladium And Deuterium, Fusion Technol., 32, 126-130 (1997).

[4] M. Swartz, Verner G., The Phusor®-type LANR Cathode is a Metamaterial Creating Deuteron Flux for Excess Power Gain, Proc. ICCF14 2, (2008), p 458; Ed D.J. Nagel and M.E.Melich, ISBN: 978-0-578-06694-3, 458, (2010); www.iscmns.org/iccf14/ProcICCF14b.pdf

[5] M. Swartz, "Consistency of the Biphasic Nature of Excess Enthalpy in Solid State Anomalous Phenomena with the Quasi-1-Dimensional Model of Isotope Loading into a Material", Fusion Technol., 31, 63-74 (1997).

[6] M. Swartz, "Metamaterial Shaped LANR-Cathodes Produce Deuteron Flux", Infinite Energy, vol 90, April (2010).

[7] M. Swartz, "Survey of the Observed Excess Energy and Emissions In Lattice Assisted Nuclear Reactions", Journal of Scientific Exploration, 23, 4, 419-436 (2009).

[8] M. Swartz, Excess Power Gain using High Impedance and Codepositional LANR DevicesMonitored by Calorimetry, Heat Flow, and Paired Stirling Engines, Proc. ICCF14 1, (2008), p 123; Ed D.J. Nagel and M.E.Melich, ISBN: 978-0-578-06694-3, 123, (2010); www.iscmns.org/iccf14/ProcICCF14a.pdf
[9] M. Swartz, G. Verner, "Excess Heat from Low Electrical Conductivity Heavy Water Spiral-Wound Pd/D2O/Pt and Pd/D2O-PdCl2/Pt Devices", *Condensed Matter Nuclear Science, Proc.ICCF-10*, World Scientific, ISBN 981-256-564-6, 29-44; 45-54 (2006).
[10] M. Swartz, Optimal Operating Point Manifolds in Active, Loaded Palladium Linked to Three Distinct Physical Regions, Proc. ICCF14 2, (2008), p 639; Ed D.J. Nagel and M.E.Melich, ISBN: 978-0-578-06694-3, 639, (2010); www.iscmns.org/iccf14/ProcICCF14b.pdf
[11] M. Swartz, Verner G., et al., Non-Thermal Near-IR Emission from High Impedance and Codeposition LANR Devices, Proc. ICCF14 1, (2008), p 343; Ed D.J. Nagel and M.E.Melich, ISBN: 978-0-578-06694-3, 343, (2010); www.iscmns.org/iccf14/ProcICCF14a.pdf
[12] M. Swartz, "Improved Electrolytic Reactor PerformanceUsing p-Notch System Operation and Gold Anodes, Transactions of the American Nuclear Association, Nashville, Tenn. Meeting, (ISSN:0003-018X publisher LaGrange, Ill) 78, 84-85 (1998).
[13] M. Swartz, "Photoinduced Excess Heat from Laser-Irradiated Electrically-Polarized Palladium Cathodes in D2O", Condensed Matter Nuclear Science, Proc. ICCF-10, eds. Peter L. Hagelstein, Scott Chubb, NJ, ISBN 981-256-564-6, 213-226 (2006).
[14] M. Swartz, Investigations of “Heat after Death”: Analysis of Factors which Determine the Tardive Thermal Power and HAD Enthalpy”, J. Cond. Matter Nucl. Sci. 31, 20-41 (2020)
[15] M. Swartz, "Can a Pd/D2O/Pt Device be Made Portable to Demonstrate the Optimal Operating Point?", Condensed Matter Nuclear Science, Proceedings of ICCF-10, eds. Peter L. Hagelstein, Scott, R. Chubb, World Scientific Publishing, NJ, ISBN 981-256-564-6, 29-44; 45-54 (2006).
[16] M.R. Swartz, Brian Ahern, Charles Haldemann and Alan Weinberg, Excess Heat is Linked to Deuterium Loss in an Aqueous Nickel LANR System, Proc. ICCF-21, Fort Collins, Co.6/3/18 (2018), J. Condensed Matter Nucl. Sci, Vol 29, 169 (2019)
[17] M Swartz, Dielectric Behavior of Ice 1H doped with Ammonia, EE and MS Thesis (Massachusetts Institute of Technology) (1971)
[18] M. Swartz, G. Verner, J. Tolleson, P. Hagelstein, Dry, preloaded NANOR -type CF/LANR components, *Current Science*, 108, 4, 595 (2015).
[19] M. Swartz, Hagelstein P.I., Demonstration of Energy Gain from a Preloaded ZrO2–PdD Nanostructured LENR Quantum Electronic Device at MIT, J. Condensed Matter Nucl. Sci. 13, (2014), p 516 www.iscmns.org/CMNS/JCMNS-Vol13.pdf
[20] M. Swartz, Incremental High Energy Emission from a ZrO_2–PdD Nanostructured Quantum Electronic Component CF/LANR, *J. Condensed Matter Nucl. Sci*. 15, p 92 (2015);
[21] M. Swartz, Verner G., *et al*., Energy Gain From Preloaded ZrO_2–PdNi–D Nanostructured CF/LANR Quantum Electronic Components, *J. Condensed Matter Nucl. Sci*. 13, p 528 (2014); www.iscmns.org/CMNS/JCMNS-Vol13.pdf
[22] M. Swartz, R., Verner, G., *et al*., Imaging of an Active NANOR®-type LANR Component using CR-39, *J. Condensed Matter Nucl. Sci*. 15, p 81 (2015);
[23] M.R. Swartz, Comparison of NANOR-type LANR Components to 238Pu as a Heat Source for Space Flight, J. Condensed Matter Nucl. Sci, Vol 29, 238 (2019)
[24] M.R. Swartz, Aqueous and Nanostructured CF/LANR Systems Each have Two Electrically Driven Modes, Proc. ICCF-21, Fort Collins, Co.6/3/18 (2018), J. Condensed Matter Nucl. Sci, Vol 29, 177 (2019)
[25] M.R. Swartz, P. Hagelstein, G. Verner, Impact of Electrical Avalanche Through a ZrO2-NiD Nanostructured CF/LANR Component on its Incremental Excess Power Gain", ICCF-19, JCMNS, 19, (2016)
[26] M.R. Swartz, "Oscillating Excess Power Gain and Coerced Magnetic Domains in M- NANOR-type CF/LANR Components", J. Condensed Matter Nucl. Sci. 22, 35-46 (2017)
[27] M. Swartz, Verner, G., *et al*., Amplification and Restoration of Energy Gain Using Fractionated Magnetic Fields on ZrO_2–PdD Nanostructured Components, *J. Condensed Matter Nucl. Sci*. 15, p 66 (2015); www.iscmns.org/CMNS/JCMNS-Vol15.pdf
[28] M.R. Swartz, Peter L. Hagelstein, Increased PdD anti-Stokes Peaks are Correlated with Excess Heat Mode, J. Condensed Matter Nucl. Sci. 24, 130-145 (2017)
[29] Swartz, M.R. "Optical Detection of Phonon Gain Distinguishes an Active Cold Fusion/LANR Component", JCMNS, 20, 29-53 (2016); www.iscmns.org/CMNS/JCMNS-Vol20.pdf

[30] M.R. Swartz, Increase of an Anti-Stokes Peak at the Cathode of an Electrically-Driven, Active Aqueous Nickel/H2O/Pt System, J. Condensed Matter Nucl. Sci., Vol 279, 22 (2018)
[31] M.R. Swartz, Active LANR Systems Emit a 327.37 MHz Maser Line, Proc. ICCF-22, J. Condensed Matter Nucl. Sci., Volume 33, pages 80-110 (2020)
[32] M.R. Swartz, FCC Vacancies in ZrO_2PdD RF are the Active LANR Site, Proc. ICCF-22, J. Cond.Matter Nucl. Sci., Volume 33, pages 126-144 (2020)
[33] M.R. Swartz, Pulsatile Superhyperfine Lines at 327.37 MHz Herald LANR Activity and Possible Mass-Energy Transfer, Proc. ICCF-22, J. Condensed Matter Nucl. Sci. , Volume 33, pages 111-125 (2020)
[34] M. Swartz, R., "Charge Transfer to Methemoglobin and Oxygen using Methylene Blue, Light and Electricity", ScD Thesis, Dept. of Electrical Engineering, MIT, Cambridge, MA, (1984).
[35] Swartz, M.R., US PATENT 4,402,318 : Method Of Inactivation Of Viruses, Bacteria, Etc. In Vitro, And Production Of Vaccines
[36] Swartz, M.R., US Patent 4,305,390 : Method For Generating Oxygen In An Excited Electronic State And Inactivation Of Microorganisms
[37] Swartz, M.R. , US PATENT 4,407,282: Method And Applicator For Generating Superoxide And Hydroxl Ions In Solution
[38] Swartz, M.R., US Patent 4,181,128: Virus Inactivation Applicator and the Like
[39] Swartz, M.R., G. A. Clark, "Electron Enhancement of Photodynamic Action, SPIE Proc. Conference on Advances in Photochemistry, Vol. 505. (1987)
[40] Swartz, M.R., L. Schnipper, A. Lewin, C. Crumpacker, "Inactivation of Herpes Simplex Viruses with Methylene Blue, Light and Electricity", Proc. of the Society of Experimental Biology and Medicine, 161, 204-209, (1979)
[41] Swartz, M.R, C. Crumpacker, "Electrical Inactivation of Herpes Simplex Viruses - Types 1 and 2", Proc. 2nd International Conference on Herpes and Cancer, (1977)
[42] Swartz, M.R, L. Schnipper, and C. Crumpacker, "Inactivation Of HSV With Photoactive Dyes, Light , And Electricity", 3rd International Conference on Herpes and Cancer 1978 Herpes Workshop p.33 (1978)
[43] Schnipper L.E., A.Lewin, M. Swartz, C.S.Crumpacker, "Mechanisms of Photodynamic Inactivation of Herpes Simplex Viruses: Comparison Between Methylene Blue, Light & Electricity and Hematoporphyrin & Light", J. Clin Invest, Vol.65, Feb.,432-438 (1980)
[44] M. Swartz, R., H. Kostron, R. Martuza, A. M. Cohen, "Ionizing Radiation and Hematoporphyrin Derivative", Int J of Rad Oncology, Biology, Physics, 9, Supp‘1, 1060, (1983)
[45] Martuza, R., M. Swartz, "Increased Levels of HPD in rat glioma following direct injection", J. Neurosurgery , March (1985)
[46] Kostron H., D. A. Bellnier, C-W Lin, M. R. Swartz, R. L. Martuza, "Distribution, retention, and phototoxicity of hematoporphyrin Derivative in a Rat Glioma - Intraneoplastic versus intraperiotoneal injection", J. Neurosurg, 64, 768-774 (1986)
[47] Kostron H., M. Swartz, D. Miller, R. Martuza, "The interaction of Hematoporphyrin Derivative, Light, and Ionizing Radiation in a Rat Glioma Model", Cancer, 57: 964-970 (1986)
[48] J. O’M Bockris, A. K. N. Reddy, "Modern Electrochemistry", Plenum Press (1970).
[49] H. H. Uhlig, "Corrosion and Corrosion Control", Wiley (1971).
[50] M. Swartz, "Dances with Protons - Ferroelectric Inscriptions in Water/Ice Relevant to Cold Fusion and Some Energy Systems", Infinite Energy, 44, (2002).
[51] M.R. Swartz, Water Is Best, Infinite Energy, 134, pp 16-29, July/August (2017)
[52] von Hippel, A., Knoll, D.B., and Westphal, W.B. 1971. "Transfer of Protons Through ’Pure’ Ice 1h Single Crystals," J. Chem. Phys., 54, 134.
[53] von Hippel,A. and Farrell, E.E 1973. Mat. Res. Bull., 8,127. von Hippel, A. "Molecular Mechanisms of Conduction and Polarization in Water Vapor, Liquid Water, and Ice, II DR MIT 1972-1973.
[54] von Hippel, A. J Chem. Phys., 54, 145, (1971)
[55] Bjerrum, N. Dansk. Mat.-Fys. Medd., 27, 32. Bjerrum, N. 1951. Dansk. Mat.-Fys. Medd., 27, 41 (1951).
[56] Bjerrum, N. 1951. Kgl. Danske Videnskab. Selskab., Met. Fys. Medd., 27,1.
[57] M.R. Swartz, Buoyant Heat Transport in Flow Calorimetry, ICCF-22, J. Condensed Matter Nucl. Sci., Volume 33, pages 268-277 (2020)

6. Appendix (Arduino Program to Collect Data)

Sketch "pHlinACTnov11M2" for Arduino Uno, pH electrode, byj48 stepper motor and ULN2003 stepper driver

```
#include "Arduino.h"
unsigned long measure2;
int ph_pin = A0; //connected to PH
// Include the AccelStepper library:
#include <AccelStepper.h>
// Motor pin definitions:
#define motorPin1 4 // IN1 on the ULN2003 driver
#define motorPin2 5 // IN2 on the ULN2003 driver
#define motorPin3 6 // IN3 on the ULN2003 driver
#define motorPin4 7 // IN4 on the ULN2003 driver
// Define the AccelStepper interface type; 4 wire motor in half step mode:
#define MotorInterfaceType 8
// Initialize with pin sequence IN1-IN3-IN2-IN4 for using the AccelStepper library with 28BYJ-48 stepper motor:
AccelStepper stepper = AccelStepper(MotorInterfaceType, motorPin1, motorPin3, motorPin2, motorPin4);
void setup() {
// Set the maximum steps per second:
Serial.begin(9600);
Serial.println ("pH Linear Actuator - Nov 11 2019 Dr. M Swartz ");
Serial.println("time(sec), pos.1-pH 1, volt1, pos.2-pH 2, volt2, pos.3-pH 3, volt3, pos.4-pH 4, volt4 pos.5-pH 5, volt5 ");
stepper.setMaxSpeed(800);
}
void loop() {
double now = millis(); //time
Serial.print(now/1000);
Serial.print(", ");
delay(1000);
int measure = analogRead(ph_pin);
int measuresum = 0;
measuresum = measuresum + measure;
delay(1000);
measure = analogRead(ph_pin);
measuresum = measuresum + measure;
delay(1000);
measure = analogRead(ph_pin);
measuresum = measuresum + measure;
delay(1000);
measure = analogRead(ph_pin);
measuresum = measuresum + measure;
delay(1000);
measure = analogRead(ph_pin);
```

```
measuresum = measuresum + measure;
double measure2 = measuresum/500.;
Serial.print(measure2);
Serial.print(", ");
double voltage = measure2*5 / 1024.0;//classic digital to voltage conversion
Serial.print(voltage, 3);
Serial.print(", ");
delay(5);
// Set the current position to 0:
stepper.setCurrentPosition(0);
// Run the motor forward at 500 steps/second until the motor reaches 4096 steps (1 revolution):
while (stepper.currentPosition() != 625) {
stepper.setSpeed(500);
stepper.runSpeed();
}
delay(3000);
measure = analogRead(ph_pin);
measuresum = 0;
measuresum = measuresum + measure;
delay(2000);
measure = analogRead(ph_pin);
measuresum = measuresum + measure;
delay(2000);
measure = analogRead(ph_pin);
measuresum = measuresum + measure;
delay(2000);
measure = analogRead(ph_pin);
measuresum = measuresum + measure;
delay(2000);
measure = analogRead(ph_pin);
measuresum = measuresum + measure;
measure2 = measuresum/500.;
Serial.print(measure2);
Serial.print(", ");
voltage = measure2*5 / 1024.0;//classic digital to voltage conversion
Serial.print(voltage, 3);
Serial.print(", ");
delay(5);
stepper.setCurrentPosition(0);
// Run the motor forward at 500 steps/second until the motor reaches 4096 steps (1 revolution):
while (stepper.currentPosition() != 625) {
stepper.setSpeed(500);
stepper.runSpeed();
}
delay(2000);
```

```
measure = analogRead(ph_pin);
measuresum = 0;
measuresum = measuresum + measure;
delay(2000);
measure = analogRead(ph_pin);
measuresum = measuresum + measure;
delay(2000);
measure = analogRead(ph_pin);
measuresum = measuresum + measure;
delay(2000);
measure = analogRead(ph_pin); measuresum = measuresum + measure;
delay(2000);
measure = analogRead(ph_pin);
measuresum = measuresum + measure;
measure2 = measuresum/500.;
Serial.print(measure2);
Serial.print(", ");
voltage = measure2*5 / 1024.0;//classic digital to voltage conversion
Serial.print(voltage, 3); Serial.print(", ");
delay(5);
stepper.setCurrentPosition(0);
// Run the motor forward at 500 steps/second until the motor reaches 4096 steps (1 revolution):
while (stepper.currentPosition() != 625) {
stepper.setSpeed(500);
stepper.runSpeed();
}
delay(3000);
measure = analogRead(ph_pin);
measuresum = 0; measuresum = measuresum + measure;
delay(2000);
measure = analogRead(ph_pin);
measuresum = measuresum + measure;
delay(2000);
measure = analogRead(ph_pin);
measuresum = measuresum + measure;
delay(2000);
measure = analogRead(ph_pin);
measuresum = measuresum + measure;
delay(2000);
measure = analogRead(ph_pin);
measuresum = measuresum + measure;
measure2 = measuresum/500.;
Serial.print(measure2); Serial.print(", ");
voltage = measure2*5 / 1024.0;//classic digital to voltage conversion
Serial.print(voltage, 3); Serial.print(", ");
```

```
delay(5);
stepper.setCurrentPosition(0);
// Run the motor forward at 500 steps/second until the motor reaches 4096 steps (1 revolution):
while (stepper.currentPosition() != 625) {
stepper.setSpeed(500);
stepper.runSpeed();
}
delay(2000);
measure = analogRead(ph_pin); measuresum = 0; measuresum = measuresum + measure;
delay(2000);
measure = analogRead(ph_pin);
measuresum = measuresum + measure;
delay(2000);
measure = analogRead(ph_pin);
measuresum = measuresum + measure;
delay(2000);
measure = analogRead(ph_pin);
measuresum = measuresum + measure;
delay(2000);
measure = analogRead(ph_pin);
measuresum = measuresum + measure;
measure2 = measuresum/500.;
Serial.print(measure2); Serial.print(",");
voltage = measure2*5 / 1024.0;//classic digital to voltage conversion
Serial.print(voltage, 3);
Serial.println("");
delay(5);
// Reset the position to 0:
stepper.setCurrentPosition(0);
// Run the motor backwards at 1000 steps/second until the motor reaches -4096 steps (1 revolution):
while (stepper.currentPosition() != -2500) {
stepper.setSpeed(-1000);
stepper.runSpeed();
}
delay(4000);
}
```